

---

# Kernelised Normalising Flows

---

**Eshant English\***

Digital Health Machine Learning  
Hasso-Plattner-Institute, Germany

**Matthias Kirchler\***

Digital Health Machine Learning  
Hasso-Plattner-Institute, Germany  
University of Kaiserslautern-Landau, Germany

**Christoph Lippert**

Digital Health Machine Learning  
Hasso-Plattner-Institute, Germany

## Abstract

Normalising Flows are generative models characterised by their invertible architecture. However, the requirement of invertibility imposes constraints on their expressiveness, necessitating a large number of parameters and innovative architectural designs to achieve satisfactory outcomes. Whilst flow-based models predominantly rely on neural-network-based transformations for expressive designs, alternative transformation methods have received limited attention. In this work, we present Ferumal flow, a novel kernelised normalising flow paradigm that integrates kernels into the framework. Our results demonstrate that a kernelised flow can yield competitive or superior results compared to neural network-based flows whilst maintaining parameter efficiency. Kernelised flows excel especially in the low-data regime, enabling flexible non-parametric density estimation in applications with sparse data availability.

## 1 Introduction

Maximum likelihood is a fundamental approach to parameter estimation in the field of machine learning and statistics. However, its direct application to deep generative modelling is rare due to the intractability of the likelihood function. Popular probabilistic generative models such as Diffusion Models [3] and Variational Autoencoders [16] instead resort to optimising the Evidence Lower Bound (ELBO), a lower bound on the log-likelihood, due to the challenges in evaluating likelihoods.

The change of variables theorem offers a straightforward and elegant solution to compute the exact likelihood for deep generative models. These models, known as normalising flows, employ invertible architectures to transform complex probability distributions into simpler ones. Normalising flows excel in efficient density estimation and exact sampling, making them suitable for various applications.

Whilst flow-based models possess appealing properties rooted in invertibility, they also impose limitations on modelling choices, which can restrict their expressiveness. This limitation can be mitigated by employing deeper models with a higher number of parameters. For instance, the Glow model [15] utilised approximately 45 million parameters for image generation on CIFAR-10 [18], whereas StyleGAN3 [13], a method that doesn't use likelihood optimisation, achieved a superior FID score with only about a million parameters.

The issue of over-parameterisation in flow-based models hinders their effectiveness in domains with limited data, such as medical applications. For example, normalising flows can be used to model

---

\*Equal contribution  
email: `firstname.lastname@hpi.de`

complex phenotypic or genotypic data in genetic association studies [9, 17]; collection of high-quality data in these settings is expensive, with many studies only including data on a few hundred to a few thousand instances. In scenarios with low data availability, a flow-based network can easily memorise the entire dataset, leading to an unsatisfactory performance on the test set. While existing research has focused on enhancing the expressiveness of flows through clever architectural techniques, the challenge of achieving parameter efficiency has mostly been overlooked with few exceptions [20]. Most normalising flows developed to date rely on neural networks to transform complex distributions into simpler distributions. However, there is no inherent requirement for flows to use neural networks. Due to their over-parameterisation and low inductive bias, neural networks tend to struggle with generalisation in the low-data regime, making them inapplicable to many real-world applications.

In this work, we propose a novel approach to flow-based distribution modelling by replacing neural networks with kernels. Kernel machines work well in low-data regimes and retain expressiveness even at scale. We introduce Ferumal flows, a kernelised normalising flow paradigm that outperforms or achieves competitive performance in density estimation for tabular data compared to other efficiently invertible neural network baselines like RealNVP and Glow. Ferumal flows require up to 93% fewer parameters than their neural network-based counterparts whilst still matching or outperforming them in terms of likelihood estimation. We also investigate efficient training strategies for larger-scale datasets and show that kernelising the flows works especially well on small datasets.

## 2 Background

### 2.1 Maximum likelihood optimisation with normalising flows

A normalising flow is an invertible neural network,  $f : \mathbb{R}^D \rightarrow \mathbb{R}^D$  that maps real data  $x$  onto noise variables  $z$ . The noise variable  $z$  is commonly modelled by a simple distribution with explicitly known density, such as a normal or uniform distribution, while the distribution of  $x$  is unknown and needs to be estimated. As normalising flows are maximum likelihood estimators, for a given data set of instances  $x_1, \dots, x_n$ , we want to maximise the log-likelihood over model parameters,

$$\max_f \sum_{i=1}^n \log(p_X(x_i)).$$

With the change of variables formula,

$$p_X(x) = p_Z(f(x)) |\det J_f(x)|,$$

where  $J_f(x)$  is the Jacobian of  $f$  in  $x$ , we can perform this optimisation directly:

$$\max_f \sum_{i=1}^n \log(p_Z(f(x_i))) + \log(|\det J_f(x_i)|).$$

The first part,  $\log(p_Z(f(x_i)))$ , can be computed in closed form due to the choice of  $p_Z$ . The second part,  $\log(|\det J_f(x_i)|)$ , can only be computed efficiently if  $f$  is designed appropriately.

### 2.2 Coupling layers:

One standard way to design such an invertible neural network  $f$  with tractable Jacobian is affine coupling layers [5]. A coupling layer  $C_\ell : \mathbb{R}^D \rightarrow \mathbb{R}^D$  is an invertible layer that maps an input  $y_{\ell-1}$  to an output  $y_\ell$  ( $\ell$  is the layer index): first, permute data dimensions with a fixed permutation  $\pi_\ell$ , and split the output into the first  $d$  and second  $D-d$  dimensions:

$$[u_\ell^1, u_\ell^2] = [\pi_\ell(y_{\ell-1})_{1:d}, \pi_\ell(y_{\ell-1})_{d+1:D}].$$

Commonly, the permutation is either a reversal of dimensions or picked uniformly at random. Next, we apply two neural networks,  $s_\ell, t_\ell : \mathbb{R}^d \rightarrow \mathbb{R}^{D-d}$ , to the first output,  $u_\ell^1$ , and use it to scale and translate the second part,  $u_\ell^2$ :

$$y_\ell^2 = \exp(s_\ell(u_\ell^1)) \odot u_\ell^2 + t_\ell(u_\ell^1).$$

The first part of  $y_\ell$  remains unchanged, i.e.,  $y_\ell^1 = u_\ell^1$ , and we get the output of the coupling layer as:

$$y_\ell = C_\ell(y_{\ell-1}) = [y_\ell^1, y_\ell^2] = [u_\ell^1, \exp(s_\ell(u_\ell^1)) \odot u_\ell^2 + t_\ell(u_\ell^1)].$$

The Jacobian matrix of this transformation is a permutation of a lower triangular matrix resulting from  $u_\ell^1$  undergoing an identity transformation and  $u_\ell^2$  getting transformed elementwise by a function of  $u_\ell^1$ . The Jacobian of the permutation has a determinant with an absolute value of 1 by default. The diagonal of the remaining Jacobian consists of  $d$  elements equal to unity and the other  $D - d$  elements equal the scaling vector  $s_\ell(u_\ell^1)$ . Thus, the determinant can be efficiently computed as the product of the elements of the scaling vector  $s_\ell(u_\ell^1)$ .

The coupling layers are also efficiently invertible as only some of the dimensions are transformed and the unchanged dimensions can be used to obtain the scaling and translation factors used for the forward transformation to reverse the operation.

Multiple coupling layers can be linked in a chain of  $L$  layers such that all dimensions can be transformed:

$$f(x) = C_L \circ \dots \circ C_1(x),$$

i.e.,  $y_0 = x$  and  $y_L = f(x)$ .

### 2.3 Kernel machines

Kernel machines [29] implicitly map a data vector  $u \in \mathbb{R}^p$  into a high-dimensional (potentially infinite-dimensional) reproducing kernel Hilbert space (RKHS),  $\mathcal{H}$ , by means of a fixed feature map  $\phi : \mathbb{R}^p \rightarrow \mathcal{H}$ . The RKHS  $\mathcal{H}$  has an associated positive definite kernel  $k(u, v) = \langle \phi(u), \phi(v) \rangle_{\mathcal{H}}$ , where  $\langle \cdot, \cdot \rangle_{\mathcal{H}} : \mathcal{H} \times \mathcal{H} \rightarrow \mathbb{R}$  is the inner product of  $\mathcal{H}$ . The kernel  $k$  can oftentimes be computed in closed form without requiring the explicit mapping of  $u, v$  into  $\mathcal{H}$ , making computation of many otherwise intractable problems feasible. In particular, as many linear learning algorithms, such as Ridge Regression or Support Vector Machines, only require explicit computations of norms and inner products, these algorithms can be efficiently kernelised. Instead of solving the original learning problem in  $\mathbb{R}^p$ , kernel machines map data into the RKHS and solve the problem with a linear algorithm in the RKHS, offering both computational efficiency (due to linearity and kernelisation) and expressivity (due to the nonlinearity of the feature map and the high dimensionality of the RKHS).

## 3 Ferumal flows: kernelising flow-based architectures

In this section, we extend standard coupling layers to use kernel-based scaling and translation functions instead. Whilst neural networks are known to perform well in large-data regimes or when transfer-learning from larger datasets can be applied, kernel machines perform well even at small sample sizes and naturally trade-off model complexity against dataset size without losing expressivity.

### 3.1 Kernelised coupling layers

We keep the definition of coupling layers in Section 2, and only replace the functions  $s_\ell$  and  $t_\ell$  by functions mapping to and from an RKHS  $\mathcal{H}$ . We have to deal with two main differences to the kernelisation of many other learning algorithms: firstly, the explicit likelihood optimisation does not include a regularisation term that penalises the norm of the prediction function. And secondly, instead of a single mapping from origin space to RKHS to single-dimensional output, we aim to combine multiple layers, in each of which the scaling and translation map from origin space to RKHS to multi-dimensional output. As a result, the optimisation problem will not be convex in contrast to standard kernel learning, and we have to derive a kernelised and tractable representation of the learning objective.

In particular, in layer  $\ell$ , we introduce RKHS elements  $V_\ell^s, V_\ell^t \in \mathcal{H}^{D-d}$  and define scaling and translation as

$$s_\ell(u_\ell^1) = \left[ \langle V_{\ell,j}^s, \phi(u_\ell^1) \rangle_{\mathcal{H}} \right]_{j=1}^{D-d} \in \mathbb{R}^{D-d} \quad \text{and} \quad t_\ell(u_\ell^1) = \left[ \langle V_{\ell,j}^t, \phi(u_\ell^1) \rangle_{\mathcal{H}} \right]_{j=1}^{D-d} \in \mathbb{R}^{D-d}.$$

We summarise  $V_\ell = [V_\ell^s, V_\ell^t]$  and  $V = [V_1, \dots, V_L]$  for the full flow  $f(x) = C_L \circ \dots \circ C_1(x)$ . Since elements  $V \in \mathcal{H}^{2L(D-d)}$  and  $\mathcal{H}$ 's dimensionality is potentially infinite, we cannot directly optimise the objective:

$$\max_V \sum_{i=1}^n p_Z(C_L \circ \dots \circ C_1(x_i)) + \log(|\det J_{C_L \circ \dots \circ C_1}(x_i)|) = L(V). \quad (1)$$

However, we can state a version of the representer theorem [28] that allows us to kernelise the objective:

**Proposition 3.1.** *Given the objective  $L$  in equation (1), for any  $V' = [V'_1, \dots, V'_L] \in \mathcal{H}^{L(D-d)}$  there also exists a  $V$  with  $L(V) = L(V')$  such that*

$$V_\ell = \sum_{i=1}^n k(\cdot, u_{\ell,i}^1) A_{\ell,i}$$

for some  $A_{\ell,i} = [A_{\ell,i}^s, A_{\ell,i}^t] \in \mathbb{R}^{2(D-d)}$ . Here,  $u_{\ell,i}^1 = \pi_\ell(C_{\ell-1} \circ \dots \circ C_1(x_i))_{1:d}$ , i.e., the first part of the permuted input to layer  $\ell$  for data point  $i$ . In particular, if there exists a solution  $V' \in \arg \max_V L(V)$ , then there's also a solution  $V^*$  of the form

$$V_\ell^* = \sum_{i=1}^n k(\cdot, u_{\ell,i}^1) A_{\ell,i}.$$

*Proof.* Let  $V' \in \mathcal{H}^{2L(D-d)}$  and  $\Phi_\ell = \text{span}\{\phi(u_{\ell,1}^1), \dots, \phi(u_{\ell,n}^1)\}$  be the space spanned by the feature maps of layer  $\ell$  inputs, and let  $\Phi_\ell^\perp$  denote its orthogonal complement in  $\mathcal{H}$ . We can then represent each element  $V_{\ell,j}^s \in \mathcal{H}$  ( $j \in \{1, \dots, D-d\}$ ) as an orthogonal sum of an element of  $\Phi_\ell$  and  $\Phi_\ell^\perp$ ,

$$V_{\ell,j}^s = \phi_{\ell,j} + \phi_{\ell,j}^\perp, \text{ with } \phi_{\ell,j} = \sum_{i=1}^n A_{\ell,i,j}^s \phi(u_{\ell,i}^1) \text{ and } \langle \phi_{\ell,j}^\perp, \phi(u_{\ell,i}^1) \rangle_{\mathcal{H}} = 0 \quad \forall i = 1, \dots, n$$

for some values  $A_{\ell,i,j}^s \in \mathbb{R}$ . In the objective (1), we only use  $V_{\ell,j}^s$  to compute  $\langle V_{\ell,j}^s, \phi(u_{\ell,i}^1) \rangle_{\mathcal{H}}$  as part of the computation of  $s_\ell(u_{\ell,i}^1)$ . But due to orthogonality, it holds that

$$\langle V_{\ell,j}^s, \phi(u_{\ell,i}^1) \rangle_{\mathcal{H}} = \langle \phi_{\ell,j} + \phi_{\ell,j}^\perp, \phi(u_{\ell,i}^1) \rangle_{\mathcal{H}} = \langle \phi_{\ell,j}, \phi(u_{\ell,i}^1) \rangle_{\mathcal{H}} + \langle \phi_{\ell,j}^\perp, \phi(u_{\ell,i}^1) \rangle_{\mathcal{H}} = \langle \phi_{\ell,j}, \phi(u_{\ell,i}^1) \rangle_{\mathcal{H}}.$$

Hence, replacing  $V_{\ell,j}^s$  by  $\phi_{\ell,j} = \sum_{i=1}^n A_{\ell,i,j}^s \phi(u_{\ell,i}^1)$  keeps the objective unchanged. The reproducing property of the RKHS  $\mathcal{H}$  now states that  $\langle \phi(u_{\ell,i}^1), \phi(\cdot) \rangle_{\mathcal{H}} = k(u_{\ell,i}^1, \cdot)$ .

Repeating this for all  $\ell = 1, \dots, L$ , all  $j = 1, \dots, D-d$  and also for translations  $t_\ell$  yields a version of  $V'$  that can be represented as a linear combination of the stated form.  $\square$

Note that, in contrast to the classical representer theorem, since the objective doesn't contain a strictly convex regularisation term that penalises the model complexity, the solution is not necessarily unique. While there may be other solutions, we know that there exists a solution that can be expressed as a linear combination of kernel evaluations, so we can re-insert this solution  $V^*$  into the objective 1. For layer  $\ell$  and arbitrary  $a \in \mathbb{R}^d$ ,

$$s_\ell(a) = [\langle V_{\ell,j}^s, \phi(a) \rangle]_{j=1}^{D-d} = \left[ \sum_{i=1}^n A_{\ell,i,j}^s k(u_{\ell,i}^1, a) \right]_{j=1}^{D-d} = \sum_{i=1}^n k(u_{\ell,i}^1, a) A_{\ell,i}^s.$$

As in the objective (1),  $s_\ell$  gets only evaluated in points  $a \in \{u_{\ell,i}^1 | i = 1, \dots, n\}$ , this simplifies to

$$s_\ell(u_{\ell,m}^1) = \sum_{i=1}^n k(u_{\ell,i}^1, u_{\ell,m}^1) A_{\ell,i}^s = A_\ell^s K(U_\ell^1, U_\ell^1)_m,$$

where  $K(U_\ell^1, U_\ell^1) = \left[ k(u_{\ell,i}^1, u_{\ell,m}^1) \right]_{i,m=1}^n$  is the kernel matrix at layer  $\ell$  and  $A_\ell^s = [A_{\ell,1}^s, \dots, A_{\ell,n}^s] \in \mathbb{R}^{(D-d) \times n}$  is the weight matrix. A similar derivation holds for  $t_\ell$ .

In total, we can kernelise the objective (1) and optimise over parameters  $A \in \mathbb{R}^{L \times n \times 2(D-d)}$  instead of over  $V \in \mathcal{H}^{2L(D-d)}$ . In contrast to neural network-based learning, the number of parameters,  $2Ln(D-d)$ , is fixed except for the number of layers (since  $d$  is usually set to  $\lfloor D/2 \rfloor$ ), but increases

linearly with the dataset size,  $n$ . This makes kernelised flows especially promising for learning in the low-data regime, as their model complexity naturally scales with dataset size and does not over-parametrise as much as neural networks.

Since the resulting objective function is not convex, optimisers targeted to standard kernel machines such as Sequential Minimal Optimisation [26] are not applicable. Instead, we optimise (1) with variations of stochastic gradient descent [14].

### 3.2 Efficient learning with auxiliary points

The basic kernelised formulation can be very computationally expensive even at moderate dataset sizes and can tend towards overfitting in the lower-data regime. In Gaussian Process (GP) regression, this problem is usually addressed via sparse GPs and the introduction of *inducing variables* [27]. In a similar spirit, we introduce *auxiliary points*. In layer  $\ell$ , instead of computing the kernel with respect to the full data  $u_{\ell,1}^1, \dots, u_{\ell,n}^1$ , we take  $N \ll n$  new variables  $W_\ell^1 = [w_{\ell,1}^1, \dots, w_{\ell,N}^1] \in \mathbb{R}^{d \times N}$  and compute the scaling transform as

$$\hat{s}_\ell(u_{\ell,m}^1) = \hat{A}_\ell^s K(U_\ell^1, W_\ell^1)_m$$

with  $\hat{A}_\ell^s \in \mathbb{R}^{(D-d) \times N}$  (analogously for  $\hat{t}_\ell$ ). We make these auxiliary points learnable and initialise them to a randomly selected subset of  $u_{\ell,1}^1, \dots, u_{\ell,n}^1$ . This procedure reduces the learnable parameters from  $2n(D-d)L$  (for both  $s_\ell$  and  $t_\ell$ ) to  $2NL$ .

In another variation we make these auxiliary points shared between layers. In particular, instead of selecting  $L$  times  $N$  points  $w_{\ell,1}^1, \dots, w_{\ell,N}^1$ , we instead only select  $W^1 = [w_1^1, \dots, w_N^1] \in \mathbb{R}^{d \times N}$  once and compute at layer  $\ell$

$$\bar{s}_\ell(u_{\ell,m}^1) = \hat{A}_\ell^s K(U_\ell^1, W^1)_m.$$

This further reduces the learnable parameters to  $2N(D-d)L + 2dN$ .

## 4 Related works

We are unaware of any prior work that attempts to directly replace neural networks with kernels in flow-based architectures. However, there is a family of flow models based on Iterative Gaussianisation (IG) [2] that utilise kernels. Notable works using Iterative Gaussianisation include Gaussianisation Flows [22] and Rotation-Based Iterative Gaussianisation (RBIG) [19]. These IG-based methods differ significantly from our methodology. They rely on kernel density estimation and inversion of the cumulative distribution function for each dimension individually and incorporate the dependence between input dimensions through a rotation matrix, which aims to reduce interdependence. In contrast, our method integrates kernels into coupling layer-based architectures. Furthermore, IG-based methods typically involve a large number of layers, resulting in inefficiency during training and a comparable number of parameters to neural network-based flow architectures. In contrast, the Ferumal flow approach of incorporating kernels can act as a drop-in replacement in many standard flow-based architectures, ensuring parameter efficiency without compromising effectiveness. Another generative model using kernels is the work on kernel transport operators [11]. Huang et al. [11] demonstrated promising results in low-data scenarios and favourable empirical outcomes. However, their approach differs from ours as they employed kernel mean embeddings and transfer operators, along with a pre-trained autoencoder.

Other works focusing on kernel machines in a deep learning context are deep Gaussian processes [4] and deep kernel learning [33, 32]. Deep GPs concatenate multiple layers of kernelised GP operations; however, they are Bayesian, non-invertible models for prediction tasks instead of density estimation and involve high computational complexity due to operations that require inverting a kernel matrix. Deep kernel learning, on the other hand, designs new kernels that are parametrised by multilayer perceptrons.

Maroñas et al. [21] integrated normalising flows within Gaussian processes. Their approach differs significantly from ours as they aimed to exploit the invertibility property of flows by applying them to the prior or the likelihood. Their combined models consist of kernels in the form of GPs but also involve neural networks in the normalising flows network, resembling more of a hybrid model.

NanoFlow [20] also targets parameter efficiency in normalising flows. They rely on parameter sharing across different layers, whereas we utilise kernels. We also attempted to implement the naive parameter-sharing technique suggested by Lee et al. [20], but we found no improvement in performance.

## 5 Experiments

We assess the performance of our Ferumal flow paradigm both on synthetic 2D toy datasets and on five real-world benchmark datasets sourced from Dua and Graff [6]. The benchmark datasets include Power, Gas, Hepmass, MiniBoone, and BSDS300. To ensure consistency, we adhere to the preprocessing procedure outlined by Papamakarios et al. [24].

**Implementation details** As previously mentioned, our architecture closely resembles RealNVP, which is a fundamental flow-based architecture. We have chosen to refrain from incorporating architectural innovations such as  $1 \times 1$  convolutions [15], which could potentially enhance the effectiveness of our architecture in creating optimal splits.

In our setting, we employ a specific permutation scheme to manipulate the data dimensions. In the first layer, we apply a fixed random permutation, followed by a reversal permutation of the data dimensions in the next layer. This scheme guarantees that all data dimensions undergo a transformation in the second layer, even when the number of layers is limited. This is advantageous compared to the scenario where a fixed random permutation is applied, which may leave some data dimensions unchanged. We refer to these two layers as a “block,” and before each block, we apply ActNorm [15] to facilitate faster convergence.

For comparison purposes, we use RealNVP and Glow as baseline models. We have also included RBIG and basic autoregressive methods, MADE [24] and MAF [24], in our evaluations (results taken from existing literature). Most autoregressive flow models outperform non-autoregressive flow models. However, they usually come with the trade-off of either inefficient sampling or inefficient density estimation, i.e., either the forward or the inverse computation is computationally very expensive.

**Training details** In our study, we utilised the Squared Exponential kernel,  $k(x, y) = \exp(-\gamma\|x - y\|^2)$ , exclusively for all experiments, with hyperparameter  $\gamma > 0$ . To select the kernel length scale, we performed a hyperparameter search; we initially defined a broader grid and conducted a basic hyperparameter search to acquire a more refined grid. Subsequently, we performed a random hyperparameter search within this finer grid. Throughout the experiments, we exclusively employed the Adam [14] optimiser, whilst adjusting the  $\beta_1$  and  $\beta_2$  parameters of the optimiser. Additionally, we decayed the learning rate either with predefined steps (StepLR) or with cosine annealing. In all the experiments, we incorporated auxiliary points as we observed that they provided better results.

We implemented Ferumal flows with the Flux library [12] in Julia, whereas we used existing implementations in Python’s PyTorch [25] for the baseline algorithms. We ran all experiments for Ferumal flows on CPUs, but all other non-kernelised experiments were trained on NVIDIA A100 GPUs. It is worth noting that we did not observe a substantial difference in runtimes between our model on CPU (Intel Xeon 3.7 GHz) and other baselines. Nevertheless, certain methods such as RBIG exhibited much longer runtimes even on an A100 GPU. For more comprehensive training details, please refer to the appendix.

### 5.1 2D toy datasets

Initially, we conducted density estimation experiments on three synthetic datasets that were sampled from two-dimensional distributions exhibiting diverse shapes and numbers of modes. Figure 1 showcases the original data distribution alongside the samples generated using the Ferumal flow paradigm and the Glow model. The re-

Table 1: Results on toy datasets. NLL in nats, lower is better

Dataset	Ours (#params)	Glow (#params)
Line	<b>-3.75 (5K)</b>	-3.15 (44K)
Pinwheel	<b>2.44 (4K)</b>	2.48 (44K)
Moons	<b>2.43 (5K)</b>	2.54 (44K)

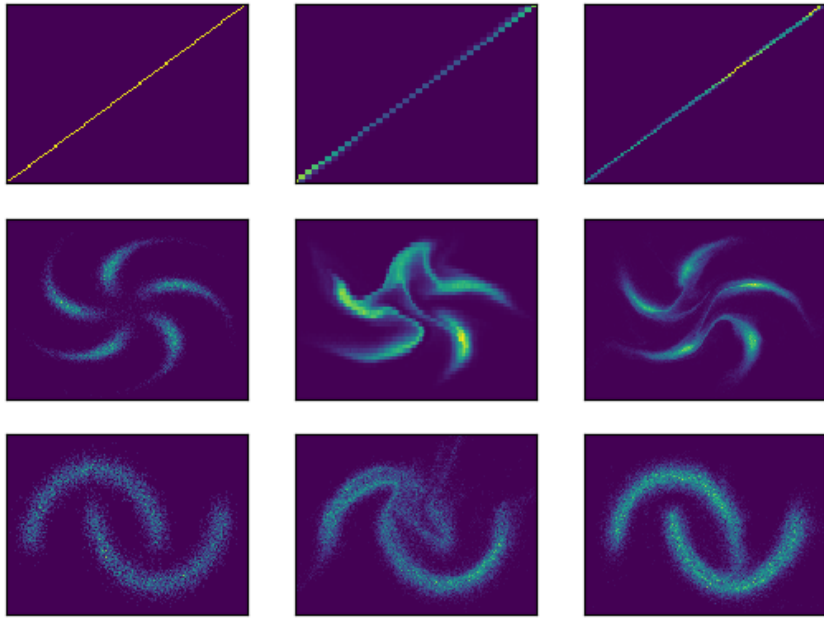


Figure 1: Histogram of 2D toy datasets. **Left:** True distribution. **Middle:** Glow. **Right:** Ours

sults demonstrate that Ferumal flows can outperform Glow on these toy datasets. All the toy datasets were trained with a batch size of 200 and for 10K iterations.

## 5.2 Real-world datasets

We conducted density estimation experiments on five UCI tabular benchmark datasets, employing the preprocessing method proposed by Papamakarios et al. [24]. In our comparisons, we included two baseline models, RealNVP and Glow, which share a similar architecture with coupling layers for efficient sampling and inference. Additionally, we also considered comparisons with RBIG, MAF, and MADE, architectures that don't use coupling layers. These methods are not directly comparable to the coupling layer-based methods, as they require significantly higher computational costs. In particular, RBIG, requires much more layers (up to 100, in our settings), whilst autoregressive flows are slow to sample from, due to their autoregressive nature.

Table 2 presents the results of our experiments, revealing that Ferumal flows consistently achieve better or competitive outcomes across all five datasets. Despite its straightforward coupling layer architecture, our approach surpasses both RBIG and MADE, and achieves similar performance than the much more expensive MAF method, underscoring the efficacy of integrating kernels.

## 5.3 Initial performance

Figure 2 presents the learning curves of the train and test loss for Ferumal flows and the two baselines. These findings demonstrate that the Ferumal flow-based architecture exhibits faster convergence compared to the neural network baselines. This expedited convergence may be due to the data-dependent initialisation of the auxiliary variables. Throughout our experiments, we maintained default settings and ensured consistent batch sizes across all models.

Table 2: Negative log-likelihood measured in nats. Smaller values are better. Results for autoregressive methods taken from the respective publications (denoted by \*).

		Datasets					
		Method	Power	Gas	Hepmass	Miniboone	BSDS300
Coupling	RealNVP	-0.17	-8.33	18.71	13.55	-153.28	
	Glow	-0.17	-8.15	18.92	11.35	-155.07	
	Ferumal Flow	<b>-0.23</b>	<b>-9.51</b>	<b>18.34</b>	<b>11.25</b>	<b>-157.01</b>	
Non-coupling	MADE*	3.08	-3.56	20.98	15.59	-148.85	
	RBIG	1.02	0.05	24.59	25.41	-115.96	
	MAF*	-0.24	-10.08	17.70	11.75	-155.69	

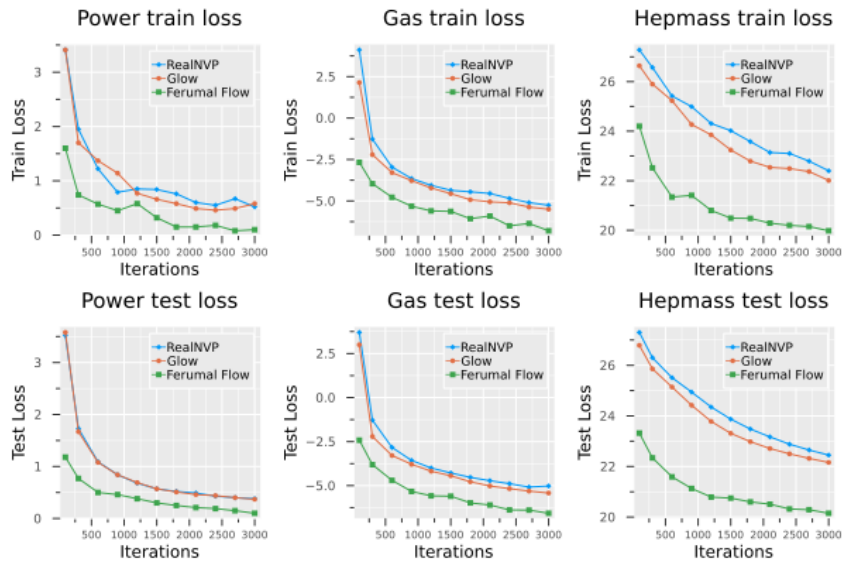


Figure 2: Negative log-likelihood (loss in nats) on training and test sets over initial training iterations.

#### 5.4 Low-data regime

In certain applications, such as medical settings, data availability is often limited. Neural network-based flows typically suffer from parameter inefficiency, leading to challenges in generalisation within low-data regimes. To assess the generalisation capability of our model under such conditions, we trained our model using only 500 examples and evaluated its performance on the same benchmark datasets. To address the challenges of limited data, we opted to tie the learned auxiliary variables across layers in this setting. This approach helped mitigate parameter complexity whilst maintaining the benefits of utilising auxiliary points.

As highlighted by Meng et al. [22], Glow and RealNVP struggled to generalise in low-data regimes, evidenced by increasing validation and test losses whilst the training losses decreased. To provide a stronger benchmark, we included the FFJORD model [8]. FFJORD is a continuous normalising flow method with a full-form Jacobian and exhibits superior performance to Glow or RealNVP in density estimation and generation tasks.

Table 3 presents the results, demonstrating that our method achieves superior generalisation. This may be attributed to the significantly lower number of parameters required compared to the continuous FFJORD method.

#### 5.5 Parameter efficiency

Table 4 shows the parameter counts of Ferumal flows against the baseline methods. Kernelising the models results in a parameter reduction of up to 93%. This reduction can be further improved by

Table 3: Results on small subset of 500 examples. NLL in nats, lower the better

Dataset	Ours (#params)	FFJORD (#params)
Miniboone	<b>27.75 (58K)</b>	39.92 (821K)
Hepmass	<b>27.90 (41K)</b>	28.17 (197K)
Gas	<b>-0.22 (11K)</b>	7.50 (279K)
Power	<b>2.91 (8K)</b>	11.33 (43K)
BSDS300	<b>-121.22 (85K)</b>	-100.32 (3,127K)

Table 4: Number of parameters

Dataset	Architectures		
	RealNVP	Glow	Ours
Miniboone	377K	395K	<b>117K</b>
Hepmass	288K	293K	<b>76K</b>
Gas	236K	237K	<b>22K</b>
Power	228K	228K	<b>16K</b>
BSDS300	458K	497K	<b>171K</b>

implementing strategies such as sharing auxiliary variables between layers or potentially with low-rank approximations, particularly in scenarios where data is limited and concerns about overfitting arise (see Appendix for additional details).

## 6 Conclusion

We have introduced Ferumal flows, a novel approach to integrate kernels into flow-based generative models. Our study highlighted that Ferumal flows exhibit faster convergence rates, thanks to the inductive biases imparted by data-dependent initialisation. Moreover, we have demonstrated that kernels can significantly reduce the parameter count without compromising the expressive power of the density estimators. Especially in the low-data regime, our method shows superior generalisation capabilities, while Glow and RealNVP fail entirely, and FFJORD lags significantly in performance.

### 6.1 Limitations and future work

In contrast to neural-network-based flows, kernelised flows require a different hyperparameter selection. In classical kernel machines, the choice of kernel usually implies a type of inductive bias (e.g., for specific data types [31]). This is not the case for our deep kernelised flows. Consequently, in this work, we focus on Squared Exponential kernels, but incorporating kernels with strong inductive biases may be a promising avenue for future research. Ferumal flows also come with other additional hyperparameters, such as the length scale of the Squared Exponential kernel or the number of inducing points. This does not increase the hyperparameter search space, though, as other hyperparameters specific to neural networks fall away (such as the number of neurons per layer).

One drawback of vanilla Ferumal flows is that their parameter count grows linearly with the number of data points, making them all but infeasible for higher data regimes. Similarly, the computational cost is quadratic in the number of data points. We provided one possible solution for this, using a limited number of auxiliary points for approximate kernel computations instead.

The present work introduces kernels only in basic affine coupling layers as introduced with RealNVPs. However, the concepts also directly apply to other coupling-layer-type networks, such as neural spline flows [7], ButterflyFlows [23], or invertible attention [30] for greater expressiveness and parameter efficiency. Ferumal flows can also be directly enhanced with other building blocks such as  $1 \times 1$  convolutions instead of permutations [15] or MixLogCDF-coupling layers [10].

Whilst our method can be applied to coupling-type flow-based architectures, it poses challenges when it comes to ResFlow-like architectures [1, 2], which require explicit control of Lipschitz properties of the residual blocks. As a result, extending our approach to ResFlow-like architectures is left as a direction for future research.

### 6.2 Broader impact

One major drawback of existing normalising flow algorithms is their dependence on an abundance of training data. The introduction of kernels into these models may allow the application of flows in low-data settings. Additionally, in the era of increasingly large and complex models, energy consumption has become a significant concern. The reduction in parameters can contribute to energy savings. Notably, our models, owing to their low parameter complexity, were successfully trained

without the need for a GPU. We anticipate that future research will continue to explore efficient methodologies and strive for reduced energy demands.

## Acknowledgments and Disclosure of Funding

We extend our gratitude to Noel Danz for his valuable discussions on coding in Julia. We would also like to express our appreciation Arkadiusz Kwasigroch, and Alexander Rakowski for their initial feedback on the draft. Additionally, we acknowledge the support provided by HPI DSE research school.

## References

- [1] J. Behrmann, W. Grathwohl, R. T. Q. Chen, D. Duvenaud, and J.-H. Jacobsen. Invertible residual networks, 2019.
- [2] S. Chen and R. Gopinath. Gaussianization. *Advances in neural information processing systems*, 13, 2000.
- [3] B. Dai and U. Seljak. Sliced iterative normalizing flows. In *International Conference on Machine Learning*, 2020.
- [4] A. C. Damianou and N. D. Lawrence. Deep gaussian processes, 2013.
- [5] L. Dinh, J. Sohl-Dickstein, and S. Bengio. Density estimation using real nvp, 2017.
- [6] D. Dua and C. Graff. UCI machine learning repository, 2017. URL <http://archive.ics.uci.edu/ml>.
- [7] C. Durkan, A. Bekasov, I. Murray, and G. Papamakarios. Neural spline flows, 2019.
- [8] W. Grathwohl, R. T. Q. Chen, J. Bettencourt, I. Sutskever, and D. Duvenaud. Ffjord: Free-form continuous dynamics for scalable reversible generative models, 2018.
- [9] D. Hansen, B. Manzo, and J. Regier. Normalizing flows for knockoff-free controlled feature selection. *Advances in Neural Information Processing Systems*, 35:16125–16137, 2022.
- [10] J. Ho, X. Chen, A. Srinivas, Y. Duan, and P. Abbeel. Flow++: Improving flow-based generative models with variational dequantization and architecture design. In *International Conference on Machine Learning*, pages 2722–2730. PMLR, 2019.
- [11] Z. Huang, R. Chakraborty, and V. Singh. Forward operator estimation in generative models with kernel transfer operators, 2021.
- [12] M. Innes, E. Saba, K. Fischer, D. Gandhi, M. C. Rudilosso, N. M. Joy, T. Karmali, A. Pal, and V. Shah. Fashionable modelling with flux. *CoRR*, abs/1811.01457, 2018. URL <https://arxiv.org/abs/1811.01457>.
- [13] T. Karras, S. Laine, and T. Aila. A style-based generator architecture for generative adversarial networks, 2019.
- [14] D. P. Kingma and J. Ba. Adam: A method for stochastic optimization. *arXiv preprint arXiv:1412.6980*, 2014.
- [15] D. P. Kingma and P. Dhariwal. Glow: Generative flow with invertible 1x1 convolutions, 2018.
- [16] D. P. Kingma and M. Welling. Auto-encoding variational bayes, 2022.
- [17] M. Kirchler, C. Lippert, and M. Kloft. Training normalizing flows from dependent data. *arXiv preprint arXiv:2209.14933*, 2022.
- [18] A. Krizhevsky. Learning multiple layers of features from tiny images. Technical report, 2009.

[19] V. Laparra, G. Camps-Valls, and J. Malo. Iterative gaussianization: From ICA to random rotations. *IEEE Transactions on Neural Networks*, 22(4):537–549, apr 2011. doi: 10.1109/tnn.2011.2106511. URL <https://doi.org/10.1109/2Ftnn.2011.2106511>.

[20] S. Lee, S. Kim, and S. Yoon. Nanoflow: Scalable normalizing flows with sublinear parameter complexity, 2020.

[21] J. Maroñas, O. Hamelijnck, J. Knoblauch, and T. Damoulas. Transforming gaussian processes with normalizing flows, 2021.

[22] C. Meng, Y. Song, J. Song, and S. Ermon. Gaussianization flows, 2020.

[23] C. Meng, L. Zhou, K. Choi, T. Dao, and S. Ermon. ButterflyFlow: Building invertible layers with butterfly matrices. In K. Chaudhuri, S. Jegelka, L. Song, C. Szepesvari, G. Niu, and S. Sabato, editors, *Proceedings of the 39th International Conference on Machine Learning*, volume 162 of *Proceedings of Machine Learning Research*, pages 15360–15375. PMLR, 17–23 Jul 2022. URL <https://proceedings.mlr.press/v162/meng22a.html>.

[24] G. Papamakarios, T. Pavlakou, and I. Murray. Masked autoregressive flow for density estimation, 2018.

[25] A. Paszke, S. Gross, F. Massa, A. Lerer, J. Bradbury, G. Chanan, T. Killeen, Z. Lin, N. Gimelshein, L. Antiga, et al. Pytorch: An imperative style, high-performance deep learning library. *Advances in neural information processing systems*, 32, 2019.

[26] J. Platt. Sequential minimal optimization: A fast algorithm for training support vector machines. 1998.

[27] J. Quiñonero-Candela and C. E. Rasmussen. A unifying view of sparse approximate gaussian process regression. *Journal of Machine Learning Research*, 6(65):1939–1959, 2005. URL <http://jmlr.org/papers/v6/quinonero-candela05a.html>.

[28] B. Schölkopf, R. Herbrich, and A. J. Smola. A generalized representer theorem. In *Computational Learning Theory: 14th Annual Conference on Computational Learning Theory, COLT 2001 and 5th European Conference on Computational Learning Theory, EuroCOLT 2001 Amsterdam, The Netherlands, July 16–19, 2001 Proceedings 14*, pages 416–426. Springer, 2001.

[29] B. Schölkopf, A. J. Smola, F. Bach, et al. *Learning with kernels: support vector machines, regularization, optimization, and beyond*. MIT press, 2002.

[30] R. S. Sukthanker, Z. Huang, S. Kumar, R. Timofte, and L. V. Gool. Generative flows with invertible attentions, 2022.

[31] S. V. N. Vishwanathan, N. N. Schraudolph, R. Kondor, and K. M. Borgwardt. Graph kernels. *Journal of Machine Learning Research*, 11:1201–1242, 2010.

[32] L. Wenliang, D. J. Sutherland, H. Strathmann, and A. Gretton. Learning deep kernels for exponential family densities. In *International Conference on Machine Learning*, pages 6737–6746. PMLR, 2019.

[33] A. G. Wilson, Z. Hu, R. Salakhutdinov, and E. P. Xing. Deep kernel learning. In *Artificial intelligence and statistics*, pages 370–378. PMLR, 2016.